STRUCTURAL CHEMISTRY

ISSN 2053-2296

Best practices in '0 K' DFT energy calculations on molecular crystal structures

Jacco van de Streek[a]* and Erin R. Johnson[b,c]*

[a]Avant-garde Materials Simulation, Alte Strasse 2, Merzhausen, 79249, Germany, [b]Department of Chemistry, Dalhousie University, 6243 Alumni Crescent, Halifax, NS, B3H 4R2, Canada, and [c]Yusuf Hamied Department of Chemistry, University of Cambridge, Lensfield Road, Cambridge, CB1 1EW, United Kingdom. *Correspondence e-mail: jacco.vandestreek@avmatsim.eu, erin.johnson@dal.ca

Received 16 April 2026
Accepted 12 June 2026

Edited by A. R. Kennedy, University of Strathclyde, United Kingdom

This article is part of the *Best practice in crystallography* series

Keywords: energy calculations; zero Kelvin; density functional theory; DFT; energy minimization; best practice.

Supporting information: this article has supporting information at journals.iucr.org/c

This article describes best practices for 'zero Kelvin' energy calculations on molecular crystals and is targeted for non-experts who would like to perform their own calculations or assess the accuracy and validity of such calculations reported in the scientific literature. The recommended computational procedure can be summarized as follows. (1) Energy optimize the crystal structures of interest with a suitable dispersion-corrected density functional, such as PBE (abbreviated here as PBE+D). (2) Based on the extent of geometric distortions after energy minimization, decide if subsequent energy calculations are required and meaningful. (3) Decide if the PBE+D crystal energies suffice; if they do not, perform a single-point energy calculation on the molecular crystal with a hybrid exchange-correlation functional, such as PBE0, again with a suitable dispersion correction. Similarly, decide if single-point energy calculations on the individual molecules with a more accurate level of theory, such as MP2D or ωB97X+D, are required to improve the molecular energies to account for multiple conformations or tautomers.

1. Introduction

Density functional theory (DFT) calculations are now a routinely used technology in applications to molecular crystals, providing valuable predictions of their structures, relative energies and other properties of interest. DFT calculations can be used for many purposes where experimental data are currently not available or cannot be obtained directly, or where there are reasons to suspect that the experimental crystal structure model may be incorrect. For example, the results from a DFT energy minimization can be used to confirm if an experimental crystal structure is stable, or to decide between multiple models differing in H-atom positions depending on their relative energies.

As hardware becomes cheaper and faster, and software becomes more efficient, increasingly many non-experts will wonder how they can use DFT calculations in their work, find themselves collaborating with computational crystallographers, or review papers reporting DFT calculations. In this article, we provide an overview of best practices and guiding principles, based on a collection of our own experiences collected over the past 30 years, the scientific literature, discussions with many experts in the field, and questions from non-experts.

As the field of DFT calculations is a vast domain, the hardest part of writing a best practices guide for a general audience is the decision of what to include. For simplicity, this article is restricted to closed-shell molecular crystal structures in their ground state in thermodynamic equilibrium that are

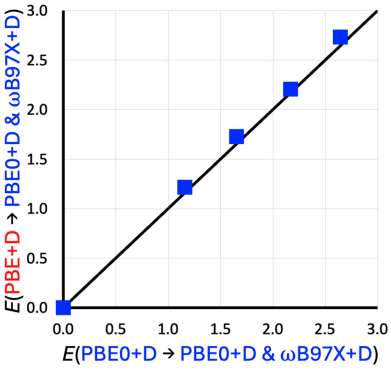

insulators. In practice, this spans most crystal structures consisting of the elements C and H, and any of B, N, O, P, S, Se, Si, F, Cl, Br and I, as well their ions (R—COO^-, R—NH_3^+, Cl^-, *etc.*), and the Na^+, K^+ and Ca^{2+} cations. Transition metals (*e.g.* Cu^{2+}, Fe^{2+}), which may have unpaired electrons, and any materials that are conductors (such as metals), require special treatment. The crystals are assumed to be ideal: there are no defects and the crystals extend to infinity in all directions. Temperature-dependent properties (*i.e.* free energies and phonons) will not be discussed, and neither will any calculation requiring the search for a global minimum (*e.g.* crystal structure prediction or conformer analysis). Energies will only be compared between systems having the same temperature, pressure and chemical composition. Only energy calculations for crystal structures and isolated molecules in a vacuum will be addressed.

As DFT calculations on molecular crystals begin with relaxation of the structures of interest, '0 K' energy minimization is described in detail. Electronic energies, even if they are not proper temperature-dependent free energies, can reveal trends and distinguish between competing models. Thus, single-point calculations on crystal structures and individual molecules, which are required to improve the calculated electronic energies after the energy minimization, are also discussed in detail. In brief, the best practices for 0 K energy calculations on molecular crystals can be summarized as: energy minimize the crystal structure with a lower-level (cheap) DFT method, then run a single-point calculation with a higher-level (more expensive) method on the crystal structure and, if required, also on the isolated molecule(s). Recommendations regarding the best choices of methods for each of these computational steps are provided. Perhaps more important than describing how to run DFT energy calculations is to explain *why* it makes sense to perform them that way. Hence, a list of guiding principles that should be considered when deciding how to apply DFT to a research question is also included. The article ends with some examples of crystallographic cases from the literature where DFT calculations could have been applied.

2. Best practices for DFT calculations

2.1. Overview

To avoid losing the main message in the details, a high-level overview of a recommended computational workflow is described in detail below, including the individual steps and their justifications.

(1) Energy optimize the crystal structures of interest with the Perdew–Burke–Ernzerhof or PBE functional (Perdew *et al.*, 1996*a*) paired with a dispersion correction (PBE+D) or another similarly reliable generalized gradient approximation (GGA). This provides a good balance between computational cost and accuracy, as PBE+D calculations are faster, but less accurate, than more sophisticated DFT methods. Except for certain very specific use cases, the unit cell should be fully optimized as part of the energy minimization.

(2) Based on the distortions after energy minimization, decide if subsequent energy calculations are required and meaningful. If the unit cell was kept fixed, a subsequent energy minimization with the unit cell allowed to fully relax (starting from the result of the energy minimization with the fixed unit cell) is probably required.

(3*a*) Decide if the PBE+D crystal energies suffice. Even if the PBE+D energies are deemed accurate enough, a subsequent single-point calculation, possibly with a larger basis set, larger k-point grid, or in the space group $P1$, can be used to detect possible problems with any of the numerical approximations in the calculation.

(3*b*) If the PBE+D crystal energies do not suffice, add a single-point crystal energy calculation with a hybrid exchange-correlation functional, such as PBE0 (Adamo & Barone, 1999), with a dispersion correction.

(3*c*) Decide if single-point energy calculations on the individual molecules, with higher levels of theory such as MP2D or ωB97X+D, are required to improve the molecular energies.

2.2. Density functional theory (DFT)

A very brief overview of DFT is given here with the aim to introduce some of the terminology and levels of approximation. In DFT, the energy E is written as a functional of the electron density $\rho(x,y,z)$: $E = E[\rho(x,y,z)]$. E can be written as a sum of several contributions, all of which are exact except for two: the exchange functional and the correlation functional, for which only approximations are known. The better the approximation, the longer the calculation typically takes. The challenge when applying DFT is, therefore, the choice of an appropriate level of approximation.

DFT functionals can be divided into roughly four levels:

(1) Local density approximation (LDA) functionals.

(2) Generalized gradient approximation (GGA) functionals, such as PBE.

(3) Hybrid functionals, such as PBE0 (pronounced 'p b e zero'). In hybrid functionals, the approximated exchange energy is improved by mixing in some amount of 'exact exchange' from Hartree–Fock theory. In global hybrid functionals, the extent of this exact exchange is a constant, usually 25% as argued based on physical grounds (Perdew *et al.*, 1996*b*), although mixing fractions of *ca* 15 to 55% may be used depending on the particular choice of functional. Alternatively, some hybrid functionals (HSE06, ωB97X, *etc.*) are range-separated, meaning that the extent of exact-exchange mixing varies depending on the electron–electron distance.

(4) More sophisticated or specialized functionals, including double-hybrid and local-hybrid functionals, which will not be discussed further here.

As the approximations made in their construction have proven to give both qualitatively and quantitatively poor results, LDA functionals should not be used in general.

The PBE functional is a GGA that is available in most DFT packages, requires relatively modest computational resources (computer time and memory) and is appropriate for the energy minimization of most molecular crystals. PBE was the

basis for the crystal structures and energies of the first four-out-of-four success rate in the 2007 crystal structure prediction blind test (Neumann *et al.*, 2008; Neumann & Perrin, 2005). Throughout this article, we write the PBE functional whenever we refer to a GGA functional because PBE is such a familiar name and it is consistently implemented in all common DFT codes. However, most GGA functionals are at least as good a choice and we have been very satisfied with the performance of the PBE, PW91 (Wang & Perdew, 1991), revPBE (Zhang & Yang, 1998) and B86bPBE (Becke, 1986) functionals paired with appropriate dispersion corrections.

Like all GGA functionals, PBE has several well-known shortcomings:

(1) It very severely underestimates the strength of attractive van der Waals interactions (London dispersion) (Johnson *et al.*, 2004).

(2) It overestimates the strengths of hydrogen bonds and halogen bonds (Gillan *et al.*, 2016; Kim *et al.*, 2019).

(3) It overestimates the stability and degree of planarity of conjugated systems (Nam *et al.*, 2021).

(4) It overestimates the stability of organic salts over acid–base cocrystals (favours proton jumps) (LeBlanc *et al.*, 2018).

(5) It gives relatively poor accuracy for the energies of breaking and forming bonds (Goerigk *et al.*, 2017).

Points 2 to 4 are all manifestations of delocalization error (Bryenton *et al.*, 2023). In practice, pragmatic solutions for overcoming these shortcomings are known for many applications.

Ad 1. The failure of most density functionals to capture the weak attractive London dispersion forces between molecules is a well-researched topic and, fortunately, an excellent solution exists in the form of dispersion corrections. There are now many available dispersion corrections from which to choose; some of the more popular ones are D2 (Grimme, 2006), D3 (Grimme *et al.*, 2010), D3(BJ) (D3 with Becke–Johnson damping; Grimme *et al.*, 2011; Johnson & Becke, 2006), D4 (Caldeweyher *et al.*, 2020), XDM (exchange–hole dipole moment model; Becke & Johnson, 2007; Otero-de-la-Roza & Johnson, 2012*b*), TS (for Tkatchenko and Scheffler; Tkatchenko & Scheffler, 2009) and MBD or MBD-nl (many-body dispersion and non-local many body dispersion; Tkatchenko *et al.*, 2012). The dispersion correction is appended to the functional (*i.e.* PBE+D3, PBE+MBD-nl, *etc.*). We have more than once observed that experimental molecular crystal structures energy minimized with PBE+D2 contracted by 8 to 12%, while none of the other dispersion corrections show this contraction, and recommend against the use of D2 for molecular crystal structures. In our experience, the newer MBD correction performs much better than the TS correction by the same authors, so we similarly do not recommend TS. We have used Neumann–Perrin (Neumann & Perrin, 2005), D3, D3(BJ), XDM and MBD-nl in our publications and, for the reproduction of experimental crystal structures, their performance is excellent. In this article, we will use the notation '+D' to indicate any of these five recommended dispersion methods.

Ad 2. The effect of overstabilizing hydrogen (and halogen) bonds on calculated crystal structures is hardly noticeable because 0 K energy minimizations already cause the unit cell to contract slightly relative to experimental single-crystal structures obtained at finite temperatures. Additionally, strong hydrogen bonds tend to be persistent across polymorphs, leading to significant error compensation; if two polymorphs have different hydrogen-bonding patterns, the error compensation will be reduced. If energy differences are important, single-point calculations with the more accurate PBE0+D functional can be performed at the PBE+D geometries to improve the predicted energetics (Hoja *et al.*, 2019). Observing that two polymorphs have different hydrogen-bonding patterns, for example, is a good reason to assume that PBE0+D single-point energy calculations are needed to improve the calculated energies. While PBE0 uses 25% exact exchange, alternative hybrid functionals including 50% exact-exchange mixing can sometimes be more reliable for systems with strong hydrogen bonding and/or halogen bonding due to mitigation of delocalization error, although they are less accurate in general (Goerigk *et al.*, 2017) and should therefore be employed with care.

Ad 3. Delocalization error is perhaps the most problematic shortcoming of the PBE functional and its effect on molecular conformational energies can be difficult to predict and detect. The typical manifestation is that a more-planar conformer with extended conjugation is overstabilized relative to a less-planar conformer that may form more favourable intermolecular interactions (Greenwell & Beran, 2020). In practice, a single-point correction on the isolated molecules with MP2D or ωB97X +D [see Beran (2025) and below] is an adequate solution, but requires relatively large computational resources, regularly for little gain in accuracy. However, there are some instances where neglect of delocalization error on conformational energies can be catastrophic in terms of polymorph ranking.

Ad 4. Accurately predicting the relative energies of crystals related by proton transfer remains an outstanding challenge for DFT. Unlike points 2 and 3, this manifestation of delocalization error cannot be addressed in a consistently reliable way even with hybrid functionals, and single-point energy calculations will not resolve the situation as the error may alter the proton positions during initial energy minimization. The special case of salt *versus* cocrystal will be discussed further in Section 6.4.

Ad 5. PBE and other GGA functionals are well known to overestimate covalent bond strengths, and this was the original motivation for the development of hybrid functionals (Becke, 1993). However, this error will not affect molecular crystal geometries significantly. In practice, it is recommended that users only compare DFT energies between crystal structures containing the same chemical compounds for maximum error cancellation. If energies must be compared for two or more tautomeric forms of a compound, accuracy can be improved using PBE0+D and/or single-molecule corrections from ωB97X+D or MP2D.

Even today, the PBE functional still offers an adequate accuracy *versus* speed compromise for energy minimization, *i.e.* for reproducing crystal *structures*, but has been proven to give incorrect *energy* rankings for experimental polymorphs of

several compounds. Even in the 0 K approximation, crystal energies are better calculated with a hybrid functional. For 0 K energies of molecular crystal structures, a single-point calculation with the PBE0+D (Adamo & Barone, 1999) or B86bPBE0+D (Price *et al.*, 2023) hybrid functional offers an excellent accuracy *versus* speed compromise.

2.3. Basis sets

In a DFT calculation, the electron density, $\rho(x,y,z)$, is approximated as a series expansion in a set of functions called basis functions. *CASTEP*, *Quantum ESPRESSO* and *VASP* are plane-wave codes, which means that they use a Fourier series to model the electron density, while *FHI-aims* uses numerical atom-centred basis functions. Both of these basis-set types are capable of excellent accuracy if sufficiently many functions are included. An exact representation of the electron density would require an infinite number of basis functions, and truncating the expansion to a finite number of functions introduces numerical errors. The more basis functions, *i.e.* the more degrees of freedom, the lower the energy. Only energies calculated with the same basis-set size should be compared or used to compute the relative energies of different crystal structures.

The size of the basis set can be viewed as the number of mathematical functions per Å^3, such that the basis-set size increases, and the energy decreases, when the unit-cell volume shrinks. The resulting driving force is called the Pulay stress or Pulay pressure. The smaller the basis set, the greater the Pulay pressure. Furthermore, the number of plane waves, the cut-off energy and the unit-cell volume are related, *i.e.* when the unit-cell volume changes either the cut-off energy or the number of plane waves must change accordingly. Because the number of plane waves is a discrete number, this may lead to sudden small jumps in the energy, which confuses the minimization algorithm. Such jumps can be prevented by keeping the number of plane waves constant, but then the basis set changes while the unit-cell volume changes and the final crystal energy no longer corresponds to the initially specified plane-wave cut-off energy. If the unit-cell volume changes significantly during the energy minimization, it may therefore be necessary to restart the energy minimization using the energy-minimized structure as the starting structure. To check if this is necessary, calculate a single-point energy on the energy-minimized crystal structure with the same settings used for the energy minimization; the energy obtained from the single-point calculation should be the same as the final energy of the energy minimization within numerical accuracy, *i.e.* $|\Delta E| < 0.05$ kcal mol^{-1}.

For energy minimizations on an individual crystal structure, or a small set of structures, a plane-wave basis set with a minimum cut-off energy of 800 eV (electron volts) is recommended. For the purposes described in this article, values over 1200 eV cannot be expected to lead to better results and should not be used. Conversely, for energy minimizations with the unit cell fixed, Pulay pressure does not play a role and such minimizations can be carried out reliably with a relatively low cut-off energy of 520 eV. One can pre-optimize the crystal structure with the unit-cell parameters fixed with a smaller cut-off energy. That energy-minimized structure can then be used as the starting point for a subsequent energy minimization, with a larger cut-off energy, in which the unit-cell parameters are allowed to relax as well. For the particular application of molecular crystal structure prediction (CSP), this cut-off energy of 520 eV is often used as a compromise between speed and accuracy since CSP requires the DFT energy minimization of possibly hundreds of crystal structures. CSP studies benefit substantially from error cancellation and single-point calculations with a larger basis set can be used to improve the energies, while the effect of temperature on the energy differences is greater than the error introduced by using a relatively small basis set for energy minimization. Note that the cut-off energy is sometimes given in Ry (Rydberg); 520 eV corresponds to about 40 Ry, 800 eV to about 60 Ry and 1200 eV to about 90 Ry. These values are appropriate for use with either ultrasoft or PAW pseudopotentials (see Section 2.5), which are generally recommended for molecular crystals; in contrast, norm-conserving potentials tend to require higher plane-wave cut-offs.

In *FHI-aims*, the available numerical atomic orbital (NAO) basis sets are referred to as 'light', 'lightdense', 'lightdenser', 'intermediate' and 'tight'. The lightdense or lightdenser basis set is a good compromise for energy minimization, while a single-point calculation with the tight basis set on the final energy-minimized structure is recommended to improve the energy. The use of NAOs makes calculations with hybrid functionals such as PBE0 feasible for molecular crystals, while the computational cost of such calculations can be prohibitive with plane-wave basis sets. Even greater efficiency can be achieved using the PBE0′ (pronounced 'p b e zero prime') implementation in *FHI-aims*, which makes use of range separation (Kokott *et al.*, 2025).

Finally, the class of Gaussian basis sets is by far the most widely used for DFT calculations on isolated molecules. Here, collections of atom-centred Gaussian functions are used to construct the orbitals and electron density. Calculations on molecular crystals with Gaussian basis sets are possible, for example, using the *CRYSTAL17* code (Dovesi *et al.*, 2018). However, small basis sets such as 6-31G* (pronounced 'six three one g star') suffer from substantial basis-set incompleteness error, resulting in a large Pulay pressure and unit-cell contraction. Use of larger sets, such as 6-31+G*, improves accuracy, but leads to linear dependencies and often inhibits self-consistent-field convergence of the DFT energies. Additionally, time-consuming counterpoise corrections are still needed to obtain reasonable energy rankings. Thus, Gaussian basis sets are ultimately not recommended for calculations on molecular crystals.

2.4. *k*-points

As a consequence of periodic boundary conditions, DFT calculations on molecular crystals involve integration over a set of '*k*-points' that span the unit cell in reciprocal (momentum) space, termed the Brillouin zone. The finer the

integer grid of *k*-points, the more accurate the numerical integration, but the more costly the calculation. In general, we recommend a *k*-point spacing of 0.07 $Å^{-1}$ or better to calculate reliable energies. Additionally, Neumann & Perrin (2005) recommend a minimum of two *k*-points in each reciprocal unit-cell direction. When comparing the energies of two closely related crystal structures, for example, a low-temperature and a high-temperature form of the same compound with very similar unit cells, one might consider ensuring that the same set of *k*-points is used for maximum error compensation.

To check if there are any problems with the number of *k*-points, a single-point energy calculation can be performed on the crystal structure (either before or after energy minimization) with and without a minimum of two *k*-points in each reciprocal unit-cell direction. The energies should be the same within numerical accuracy, *i.e.* $|\Delta E| < 0.05$ kcal mol^{-1}. Similarly, to check if there are any problems with the *k*-point generation caused by the space-group symmetry, one can perform a single-point energy calculation with the same settings on the crystal structure converted to the *P*1 space group. Finally, because the set of *k*-points depends on the reciprocal unit cell, it is also possible that the number of *k*-points required after energy minimization is different from the initial set. It may therefore be necessary to restart the minimization with an updated starting structure if recalculating the single-point energy of the energy-minimized structure with an updated *k*-grid does not give the same result as the final energy of the minimization to within numerical accuracy.

2.5. Core electrons and relativistic effects

The electrons in an atom can be divided into the valence electrons, which determine the chemistry (as well as the structures and energies of most molecular crystals), and the core electrons. The properties of the core electrons depend almost exclusively on the element and are otherwise relatively constant across chemical compounds. Moreover, for the purpose of DFT energy calculations, the core electrons are much more difficult to model than the valence electrons (particularly with plane-wave basis sets) due to the need to accurately describe the nuclear 'cusps'. This has led to two approaches to deal with the core electrons: (i) model them explicitly or (ii) precalculate their electron-density contributions and store them in a file. The first option is implemented in 'all-electron' codes such as *FHI-aims*, while the second option is standard in plane-wave codes such as *CASTEP*, *Quantum ESPRESSO* and *VASP*, and is referred to by names such as the 'pseudopotential' or 'effective core potential' approach.

A pseudopotential can be thought of as a sphere centred at the nucleus; the electron density inside the sphere is precomputed, while the electrons outside the sphere are treated explicitly. The radius of the sphere can be varied, and the extent to which the core electrons are treated explicitly is referred to as 'soft' or 'hard'. The harder the pseudopotential, the smaller the sphere and the more of the explicit character of the core electrons is preserved. When the core electrons are not treated explicitly, the nucleus and its core electrons can be considered as a unit to which the valence electrons are added. In that picture, the nucleus plus its core electrons is sometimes referred to as an 'ion'. Using that terminology, a paracetamol molecule, for example, consists of 20 ions plus the valence electrons.

Several types of pseudopotentials are commonly used, including frozen-core potentials, norm-conserving pseudopotentials, ultrasoft core potentials and PAW (Projector-Augmented Wave) potentials. The latter two categories are used in the vast majority of computations on molecular crystals, for which the default settings or recommendations of the particular DFT software are usually sufficient. GIPAW (Gauge-Including Projector Augmented Wave) potentials are required for solid-state NMR calculations, in which the core electrons play a prominent role, although this is beyond the scope of the present article.

The closer the electrons are to the nucleus and the heavier the element, the greater the effect of relativistic corrections. For the light elements that form most organic molecules, relativistic corrections are unnecessary for the reproduction of crystal structures or for energy differences. However, such corrections are needed for heavier elements, such as Br or I atoms. In plane-wave DFT calculations (*CASTEP*, *Quantum ESPRESSO*, *VASP*, *etc.*), scalar relativistic effects are included automatically through the pseudopotential. However, in all-electron codes, such as *FHI-aims*, an explicit relativistic correction must be used. Specifically, when an element heavier than Ca (atomic number 20) is present, *FHI-aims* forces the use of the ZORA (for Zeroth-Order Regular Approximation) relativistic correction. Because energies can only be compared if the treatment of relativistic effects is consistent, and because the additional computational resources required are negligible, it is strongly recommended to always use ZORA in *FHI-aims* (include 'relativistic atomic_zora scalar' in the control.in input file).

2.6. Energy definition and single-point calculations

There are many specific quantities to which the vague general term 'energy' can refer. The energy that is routinely reported by quantum-mechanical (QM) programs is the 'electronic energy', which we write as *E* throughout this article. Whereas quantities like temperature, volume and mass have a natural zero point, energies do not, meaning that only energy *differences* can be determined. Hence, the electronic energy reported by QM software is the electronic energy with respect to a fixed, but arbitrary, reference point, which is most often the energy of the electrons and atomic nuclei at infinite separations. The formation of molecules from separated electrons and nuclei always releases large amounts of energy, so all molecules and crystal structures have large negative electronic energies, with their magnitude proportional to the number of electrons in the system. Calculating the electronic energy of a crystal structure as is, without any changes to

atomic coordinates or the unit cell, is referred to as a single-point energy or a single-point calculation. An energy minimization is made up of a series of single-point calculations.

It is also possible to calculate enthalpies and Gibbs or Helmholtz 'free energies' with quantum-mechanical software, but these are much harder to compute and will not be discussed further here. Because of the missing temperature-dependent contributions, electronic energies are often referred to as '0 K' (zero Kelvin) energies; however, experimental energies at 0 K include the zero-point energy (ZPE), which is not included in the electronic energy. As a result, even electronic energy differences obtained from QM software cannot be directly compared to relative experimental energies, because no temperature-dependent contributions and no zero-point energies are included.

The electronic energy is the energy of the entire unit cell, and so is a combination of the intra- and intermolecular interactions. The 'crystal energy' is this electronic energy normalized per mole of molecules (*i.e.* to kcal mol^{-1} or kJ mol^{-1}). The 'lattice energy' can be calculated from the crystal energy by subtracting the individual isolated molecular energies:

$$E_{\text{lattice}} = E_{\text{crystal}} - \frac{1}{N}\sum_{i=1}^{N} E_{\text{molecule},i} \qquad (1)$$

where the sum runs over all N molecules in the unit cell.

In *FHI-aims*, which uses atom-centred basis sets, the energy of an isolated molecule can be calculated directly. However, in plane-wave codes such as *CASTEP*, *Quantum Espresso* and *VASP*, calculations can only be performed on periodic structures. Thus, the energy of an isolated molecule can only be calculated by embedding it in a vacuum by defining a contrived crystal structure (in $P1$ symmetry) with very large unit-cell parameters to reduce the interaction between periodic copies. Alternatively, a series of calculations using increasingly larger unit cells can be conducted, and the energy of the molecule in an infinitely large unit cell can be obtained by extrapolation. If the isolated molecule has a net charge, this must be set in the input file for the calculation to ensure that the number of electrons is correct. For periodic-boundary calculations, a compensating background charge is automatically added for charged molecules to prevent divergence of the electrostatic component of the energy.

Molecular energies from single-point energy calculations in vacuum, using molecular geometries taken from a crystal structure. can therefore be used to calculate the intermolecular component of the lattice energy as per Equation (1). This approximation assumes rigid molecules and can be useful to identify trends for flexible molecules. However, the molecular energies should properly take into account the relaxation of the molecule upon being excised from the crystal structure (due to the accompanying loss of packing forces), and the fact that the most favourable molecular conformation may be completely different from that found in the crystal (Thompson & Day, 2014). A simple example of this is oxalic acid, in which the proton positions will differ between the crystal and the gas-phase molecule to ensure stronger intramolecular hydrogen bonding in the latter case. For more sophisticated energy calculations on individual molecules, the articles by Bursch *et al.* (2022) and Chattopadhyay *et al.* (2025), and references therein, are good starting points.

Table 1
Relative PBE+D single-point energies for a set of crystal structure models for axitinib Form XLI (CSD refcode VUSDIX04) obtained from different energy-minimization protocols.

Energy-minimization protocol	Single-point energy (kcal mol^{-1})
As published, no minimization	308.4
X—H normalized, no minimization	10.54
Energy minimized, unit cell fixed	0.30
Energy minimized, unit cell free	0.00
$<\|\Delta E\|>^1$	0.85

Note: (1) average of the ten PBE+D energy differences between the five known axitinib polymorphs (I, IV, VI, XXV and XLI) after full energy minimization.

2.7. Energy minimization

'Energy minimization' refers to a local minimization of the electronic energy with respect to changes in atomic positions and lattice parameters (unit-cell lengths and angles), *i.e.* to the nearest local minimum on a very high-dimensional potential energy surface. Note that the energy minimization cannot break symmetry to lower the energy if space-group symmetry is imposed, meaning that it may be possible to geometry optimize to 'saddle points' instead of local minima in rare cases. It is also possible that the crystal structure has higher symmetry after energy minimization (Hempler *et al.*, 2017).

The energy minimization process consists of a series of single-point calculations (as well as evaluation of the forces and stresses) on increasingly low-energy crystal structure models until some specified convergence criteria are satisfied and the optimization stops. As this process requires several, generally dozens, of successive single-point calculations, it should therefore use a relatively cheap DFT method. 'Geometry optimization' or 'geometry relaxation' are common terms used as alternatives for energy minimization. While energy minimization is sometimes referred to as 'geometry minimization', this is incorrect as the atomic coordinates are not made smaller.

Energy minimization ensures that experimental crystal structures (from any of single-crystal, powder diffraction, X-ray, neutron or electron diffraction data), manually created alternative crystal structure models (in case of ambiguities in the experimental data) and *in silico* crystal structures from CSP studies are all treated on an equal footing. This is an example of the Anna Karenina principle: there exists only one unique energy-minimized crystal structure model (with a particular DFT method and basis) for a given polymorph, but an infinite number of models that do not correspond to the energy-minimized crystal structure, each with its own crystal energy (Fig. S1 in the supporting information). Checking if two crystal structures correspond to the same polymorph (at 0 K) is also facilitated by energy minimization (Sacchi *et al.*, 2020).

The influence of omitting parts of the geometry optimization protocol on the crystal energy is shown in Table 1 for

axitinib Form XLI determined at room temperature [Cambridge Structural Database (CSD) (Groom *et al.*, 2016) refcode VUSDIX04; Campeta *et al.*, 2010]. The average energy difference between any two of the five known axitinib polymorphs (0.85 kcal mol^{-1}) is included for comparison. The shortened X—H bond lengths present in the experimental single-crystal X-ray structure account for *ca* 300 kcal mol^{-1} of destabilization; obviously, this value depends on the number of X—H bonds and, for paracetamol (CSD refcode HXACAN07; Nichols & Frampton, 1998), the corresponding destabilization is 'only' 69.7 kcal mol^{-1}. Even after correcting the short X—H distances, energy minimization lowers the energy by *ca* 10 kcal mol^{-1}, an order of magnitude more than the average energy difference between two polymorphs. In short, in order for the comparison of calculated energy differences to be meaningful, the crystal structure models must be energy minimized first.

Energy minimization also offers the opportunity to assess how well the DFT method reproduces the input crystal structure model, identifying possible issues with the proposed crystal structure, or with the choice of functional or basis set, before progressing to single-point energy calculations with higher levels of theory. If the crystal structure distorts substantially during the relaxation, it is likely incorrect and there is no value in performing additional single-point calculations. In approximate order of importance, experimental structures can distort during energy minimization for the following reasons.

(1) Incorrectly positioned or missing H atoms. Due to their low X-ray scattering power, H atoms are sometimes positioned incorrectly, even in single-crystal X-ray structures. Incorrect models contain large internal strains and stresses that can trivially be detected by relaxing the unit cell as part of the energy minimization and seeing the unit cell deform.

(2) If the crystal structure has been determined from powder diffraction data, functional groups having a similar electron-density distribution may have been swapped. For example, N and C—H represent the same number of electrons and may be exchanged without it being noticeable in the Rietveld refinement. Real-space structure solution algorithms may not explore all ring conformations of flexible rings, and a published structure may reflect the input conformation rather than the optimal ring conformation.

(3) Disorder. The crystal structure model resulting from a diffraction experiment records a space and time average, and disorder can be hidden in the anisotropic displacement parameters (ADPs). This is illustrated in Fig. S2 for CSD refcode ANOCOW01 (Zouev *et al.*, 2011). If the ADPs are ignored, the propyl chain is incorrectly interpreted as a propenyl chain due to the short distances between the disordered C atoms when their positions are averaged. Only after the large ADPs have been split into pairs of disordered atoms, and the space-group symmetry broken, can the two underlying individual propyl chains be resolved.

(4) Temperature effects other than disorder. If an experimental crystal structure was determined at a relatively high temperature, it may be distorted relative to the '0 K' energy-minimized structure. If the source of distortion is a temperature effect, it should be possible to confirm this by determining the crystal structure at a lower temperature (Bond *et al.*, 2011).

(5) Inaccuracies in the computational methods used. For example, due to Pulay pressure, a decent basis set must be used when energy minimizing crystal structures with the unit cell free to relax. The approximations inherent in PBE+D may affect calculated relative energies of a set of crystal structures, but hardly ever lead to distortions in the energy-minimized structures themselves; however, there are some rare exceptions. In 2014, we observed a space-group change from $C2/m$ to $R\bar{3}m$ upon energy minimization with PBE+D for one of the polymorphs of butyne [van de Streek & Neumann (2014); CSD refcode BUTYNE01 (Ibberson & Prager, 1995)] due to a shift of the layers during the energy minimization that we could not explain. With PBE0+D, the crystal structure of butyne is reproduced without any layer shift and the space group remains $C2/m$ (Fig. S3). Such failures of PBE+D are rare and we have never observed any failure for large molecules without molecular symmetry, such as pharmaceutical compounds.

(6) Unknown reasons. The crystal structure of Form E of crystal structure prediction blind test compound XXIII [CSD refcode XAFPAY04 (Samas, 2016); *CSD Communication*, doi:10.5517/cc1kl8dt], distorts when energy minimized with PBE+D (Fig. S4) or PBE0+D, but we have not been able to find a structural model that explains this behaviour.

Incorrect H-atom positions, disorder and minor errors in crystal structures determined from powder diffraction data are not uncommon and affect perhaps one in ten energy minimizations. The remaining three reasons are rare, and less than 1% of energy minimizations are affected by them.

An exception is spurious proton transfer upon energy minimization with a GGA functional such as PBE, which can be regularly observed. When proton transfer is observed, the energy of the crystal structure can no longer be calculated with any degree of accuracy. The positions of the non-H atoms, however, are not affected, and since all measures to compare crystal structures described in Section 4 are almost exclusively determined by the positions of the non-H atoms, measures based on crystal structure (as opposed to crystal energy) can still be used.

2.8. Convergence

During geometry optimization, the energy changes between successive minimization steps are monitored, as well as the changes to the atomic coordinates and the unit-cell parameters. When the changes are all smaller than certain pre-set criteria, it is assumed that further minimization steps will have negligible effects on the energy, atomic positions and lattice constants, and the energy minimization is taken to be completed or 'converged'. Usual convergence criteria are, for example, limits of 0.005 kcal mol^{-1} on the energy difference between successive minimization steps, 0.003 Å on the largest Cartesian displacement and 0.7 kcal mol^{-1}/Å on the largest force.

Setting a maximum number of steps is a common safety mechanism to prevent wasting resources on an energy minimization that is undergoing large geometric changes, which indicates that the starting model was probably far from optimal or even wrong (for example, due to missing or extra H atoms). If a maximum number of minimization steps has been set, it is important to check that the minimization completed because the convergence criteria were met and not because the step limit was reached. The chosen step limit may need to be exceeded in cases where the optimization is slow to converge, for example, due to a fairly flat potential energy surface, which may occur for crystal structures with π-stacked molecular layers for example. In contrast, the minimization algorithm is occasionally unable to determine which changes should be made to the crystal structure to decrease the energy and effectively gets 'stuck', such that successive changes cause the energy to oscillate; the minimization ultimately aborts when the step limit is reached without having achieved convergence. In these cases, the lack of progress can be difficult to distinguish from regular convergence as the minimization may appear to have finished normally. Indeed, literature reports of two successive equivalent DFT energy minimizations resulting in different energy minima (*e.g.* Hodge *et al.*, 2020) might be explained by assuming that the first minimization terminated prematurely, before reaching convergence. If it is suspected that the energy minimization terminated before proper convergence, it might be sufficient to start the minimization from scratch taking the semi-optimized crystal structure as the starting point. In cases where the minimization becomes stuck and continuing from the last geometry is insufficient, it may also help to pre-optimize the crystal structure with slightly different settings, for example, with the unit cell kept fixed or with a different dispersion correction.

2.9. Including pressure

Simulating the effect of pressure is easy and requires negligible computational resources: all that is needed is the addition of a pressure–volume (PV) term during the energy minimization. This corresponds to an isotropic pressure, often referred to as 'hydrostatic pressure'. It is also possible to apply anisotropic pressures by specifying the applied pressure as a tensor that is entered as a 3×3 matrix; entering any multiple of the identity matrix is equivalent to applying a hydrostatic pressure. The effect of standard atmospheric pressure, *ca* 0.0001 GPa, on crystal structures and their relative energies is negligible, but the effect of pressure becomes significant above 0.1 GPa. For example, Fig. S5 shows the effect of a 4.0 GPa applied pressure on the crystal structure of paracetamol (CSD refcode HXACAN12; Boldyreva *et al.*, 2000), which can be reproduced very well by DFT calculations.

2.10. Hardware and software considerations

The main bottleneck when running quantum-mechanical calculations is memory (RAM), which is why DFT calculations are best run on a High-Performance Computing (HPC) cluster where the calculations can be parallelized over multiple CPUs, increasing the amount of RAM available for the calculation and reducing the wall-clock time. Most energy minimizations with the PBE+D functional, which is a useful complementary technique when solving crystal structures from powder diffraction data, can be run on a high-end PC, which at the time of writing is, for example, a 16-core Xeon w5 with 64 GB DDR5 RAM and a Solid State Drive (SSD).

Table 2
Licensed and unlicensed features in *Mercury*.

Feature	Free *Mercury*	Licensed *Mercury*	JvdS′ github repository[1]
Adding H atoms	**X**	**X**	
Overlay structures		**X**	
Visualize hydrogen bonds	**X**	**X**	
Normalize **X**—H bonds		**X**	**X**
Calculate RMSCDs		**X**	**X**
Calculate void space		**X**	**X**
Reduce centred cells	**X**	**X**	**X**
Convert to *P*1	**X**	**X**	**X**
Simulate PXRD	**X**	**X**	**X**
De Gelder's PXRD similarity measure		**X**[2]	**X**
Split disorder ADPs	(**X**)[3]	(**X**)[3]	**X**
Reduce orthogonality defect	**X**[4]	**X**[4]	**X**

Notes: (1) https://github.com/JvdS147/ComputationalCrystallographersAnonymous, open-source, C++, can be compiled on Windows, Linux and MacOS. (2) In the 'Searches' panel under 'Options' | 'Customize Columns' add 'PXRD similarity'. (3) A feature request has been sent to the Cambridge Crystallographic Data Centre. (4) Implicit in the 'Transform to Reduced Cell' command.

As early as 2016, a validation across different DFT packages implementing different types of basis sets and different numerical methods demonstrated that all provided consistent results (Lejaeghere *et al.*, 2016). Although there may be differences in the resources required, 0 K energy minimizations with PBE+D and single-point calculations with PBE0+D are now routine, and the final crystal structures and energy differences should be the same independent of the DFT software used. We do note that the electronic energy does not have a unique zero point, so that only relative energies and not absolute energies should be directly compared in most cases. While there are occasional reports in the literature of equivalent DFT energy minimizations resulting in different energy minima (*e.g.* Hodge *et al.*, 2020), this is likely due to an insufficiently tight convergence setting for one of the energy minimizations (*i.e.* one of the minimizations aborting prematurely without having reached the local minimum), which could have been overcome with a little trial and error. For the more than one thousand energy minimizations that we have published thus far, we have used the *CASTEP* (Clark *et al.*, 2005), *VASP* (Kresse & Furthmüller, 1996; Kresse & Hafner, 1994) and *FHI-aims* (Blum *et al.*, 2009) codes with great satisfaction, but this should not be considered a recommendation against other DFT softwares.

3. Best practices for input crystal structures

3.1. Preparing input files, H atoms, disorder and fractional occupancies

The CIF file format can be complicated and not all programs may be able to read all CIF files. We have found that the

free version of *Mercury* (Macrae *et al.*, 2020), which is available for Linux, MacOS and Windows, saves very short clean CIF files that can be interpreted by all programs we have ever used (Table 2). For molecules at special lattice positions, be careful about the distinction between the asymmetric unit and the expanded molecule; the latter is the default in *Mercury*. The free and open-source *critic2* code (Otero-de-la-Roza *et al.*, 2014*b*) is useful for converting CIF files to the appropriate input file formats used by most popular QM codes.

By far the most common problems with experimental crystal structures relate to H atoms, which may be missing or not form the correct hydrogen-bonding pattern. The automatic addition of missing H atoms in *Mercury* should add H atoms bonded to C atoms correctly, but –OH H atoms are added in a random orientation and may have to be repositioned manually. When an incorrect number of H atoms is present, the QM calculation still assumes an overall neutral charge, which can result in dangling bonds. In such cases, the only sign that something is wrong with the structural model might be convergence problems due to a vanishing band gap that results from performing a spin-restricted calculation on a system with unpaired electrons.

Disorder remains one of the hardest features of molecular crystals to treat computationally. While QM programs do not allow fractionally occupied atoms to match the fractional occupancies in disordered molecular crystal structures, disordered atoms can be correlated. Thus, even if fractional occupations were possible, a model in which electrons interact with the average electron density of the disordered atoms would lead to incorrect crystal energies. It is, however, straightforward to write separate CIF files for the major and minor components of a disordered crystal structure using *Mercury*. In more complicated cases, preparing crystal structure models suitable for energy calculations may require breaking the space-group symmetry, *e.g.* if an infinite chain of hydrogen bonds is propagated across twofold axes or inversions; see CSD refcode ARUFIE (Tejchman *et al.*, 2015) for an example.

For non-stoichiometric hydrates, it is often possible to construct structural models with fully occupied atoms that approximate the experimental stoichiometry and that lead to acceptable atomic coordinates and unit-cell parameters. However, we are not aware of a generally applicable method to calculate their energies and the configurational entropy contribution to their free energies, and such calculations are beyond the scope of the present article.

Overall, the effect of disorder on the atomic coordinates, unit-cell parameters, electronic energies and configurational entropy contribution to the free energies must be carefully investigated on a case-by-case basis. After many years of research into this topic, we wrote a comprehensive guide to the calculation of the structures, energies and free energies of disordered molecular crystal structures, which is to be submitted in the near future (van de Streek *et al.*, 2026).

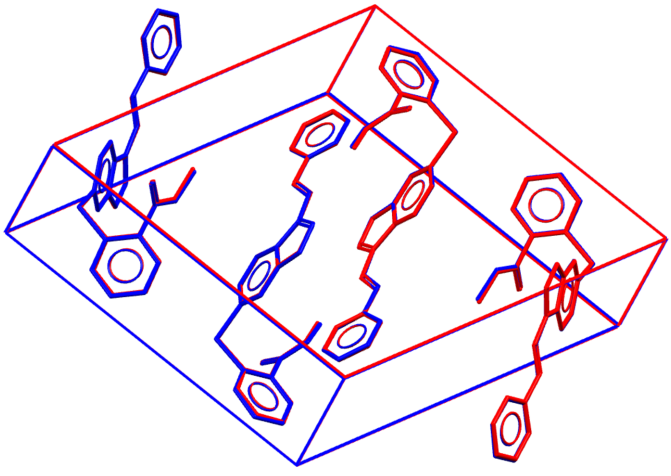

Figure 1
Overlay of the experimental crystal structure of Form XLI of axitinib at room temperature (red) and the same structure after energy minimization with PBE+D (blue). The *FHI-aims* result with PBE+MBD-nl/light-dense is shown, yielding an RMSCD = 0.059 Å.

3.2. Normalize the *X*—H bond lengths

The electron density of H atoms is usually displaced towards the non-H atom to which it is bonded. Thus, the positions of the electron-density maxima and the H-atom nuclei do not coincide and are typically about 0.1 Å apart. As crystallographers tend to position the H atoms at the electron-density maxima, the *X*—H bond lengths are about 0.1 Å too short in most experimental single-crystal structures. This leads to strong forces, large atomic displacements and large energy changes in the initial stages of the energy minimization, which serve no other purpose than to position the H atoms correctly. Convergence of the energy minimization can, therefore, be accelerated by normalizing the *X*—H bond distances in the input structure to match the values found from neutron diffraction experiments, which measure the nuclear positions.

3.3. Choice of unit cell

The choice of unit cell is extremely important in QM calculations on periodic systems as it will affect the computational cost and smoothness of convergence in the energy minimization. In particular, the more orthogonal the unit-cell axes are, the less they correlate and the more numerically stable the calculations can be expected to be. Thus, while crystallographers tend to prefer standard space-group settings over orthogonality of unit-cell axes, transformation to a non-standard setting may improve convergence by reducing linear dependencies. Let us consider the crystal with CSD refcode CUKGAR01 (Feast *et al.*, 2009) as an example. When refined in the standard setting of $P2_1/c$, it has a unit-cell angle β = 132.04°, while transformation to the non-standard setting of $P2_1/n$ results in β = 92.00° and reduces the correlation between the *x*- and *z*-coordinates. Selecting an appropriate set of *k*-points is also easier when the unit cell is as orthogonal as possible, and very acute or obtuse angles may lead to more *k*-points than necessary, increasing the computational resources. It is therefore recommended to make all unit-cell

angles as close as possible to 90° before energy minimizing a crystal structure.

A related consideration is the greater the unit-cell volume, the greater the required computational resources. This means that centred unit cells can be reduced to primitive unit cells to speed up the DFT calculations, which can be especially useful for R- and F-centred unit cells. However, standard transformation matrices may lead to very acute or very obtuse unit-cell angles, so some trial and error may be needed in practice.

For example, consider the crystal structure of the 1,2,4-tribromobenzene isomer (CSD refcode UYUQAJ; Bujak *et al.*, 2021), which has a space group of *Fdd*2 with a unit-cell volume of 9313 Å^3. Conversion to a primitive unit cell using the transformation matrix [0 $\frac{1}{2}$ $\frac{1}{2}$, $\frac{1}{2}$ 0 $\frac{1}{2}$, $\frac{1}{2}$ $\frac{1}{2}$ 0] leads to a volume of 2328 Å^3 and a very acute angle of β = 20.6°. A subsequent transformation using the matrix [$\bar{1}$ $\bar{1}$ 1, $\bar{1}$ 0 1, 0 1 $\bar{1}$] reduces the orthogonality defect and gives unit-cell angles of 90.38, 92.86 and 82.36°, all close to 90°. However, after the second transformation, the matrix representation of one of the symmetry operators is [1 1 $\bar{1}$, 0 $\bar{1}$ 0, 0 0 $\bar{1}$], which is not one of the 64 standard representations and may, therefore, lead to error messages in crystallographic programs. If non-standard matrix representations cause problems, the space group can be reduced to *P*1 or *P*$\bar{1}$ (if the original space group contained an inversion at the origin). Conversion to a lower-symmetry space group will not usually affect the energy minimization, except for some crystal structures that undergo reversible phase transitions as a function of temperature. In almost all such cases, the high-temperature (HT) phase has the higher space-group symmetry, such that a '0 K' energy minimization of the HT phase in *P*1 or *P*$\bar{1}$ may convert to the low-temperature phase. Note that the HT phase should be less stable at 0 K and its higher minimized energy, caused by the fewer degrees of freedom in the imposed space-group symmetry, is not an artefact.

If multiple experimental crystal structures are available, the structure determined at the lowest temperature should be the easiest to energy minimize with the unit cell free because the calculations reflect the unit-cell volume at 0 K. All other experimental determinations of the same polymorphs should trivially converge to the same energy-minimized structure, but probably at the cost of requiring more minimization steps due to the greater adjustment of the unit-cell volume that is needed.

4. Comparing crystal structures

Before using the energy-minimized crystal structure for energy calculations, it is important to confirm that the crystal structure has not distorted too much as a result of the energy minimization. If the structure distorted considerably, something is likely wrong and it should not be carried forward to further energy calculations. Many methods are available to compare the initial and the energy-minimized crystal structure (Mayo & Johnson, 2025), but the two simplest options are (i) visually through an overlay or (ii) by calculating the Root-Mean-Square Cartesian Displacement (RMSCD).

Mercury can be used to create visual structure overlays. Fig. 1 shows the overlay of the experimental crystal structure of form XLI of axitinib and the corresponding energy-minimized PBE+D structure. We selected red (warm) for the experimental crystal structure, which includes thermal effects, and blue (cold) for the calculated '0 K' structure. A black background is environmentally unfriendly in case the document is printed, so a white or transparent background is recommended. The high quality of reproduction between the experimental and energy-minimized crystal structures shown in Fig. 1 is routinely achievable with PBE+D.

The quantity used for comparison of experimental and energy-minimized crystal structures is the RMSCD, excluding H atoms. 'Cartesian displacement' is not uniquely defined when the unit cells of the two crystal structures to be compared are different, as is the case when the lattice parameters are allowed to vary in the energy minimization. In this work, the Cartesian displacement for an atom in two crystal structures (1) and (2) is defined as (see Neumann & Perrin, 2005).

$$\text{Cartesian displacement} = \left(\left|\mathbf{G}_1 \cdot \mathbf{r}_1 - \mathbf{G}_1 \cdot \mathbf{r}_2\right| + \left|\mathbf{G}_2 \cdot \mathbf{r}_1 - \mathbf{G}_2 \cdot \mathbf{r}_2\right|\right)/2 \quad (2)$$

where $\mathbf{r}_i$ are the fractional coordinates of the atom in crystal structure *i* and $\mathbf{G}_i$ is the transformation matrix from fractional to Cartesian coordinates for crystal structure *i*. This definition of Cartesian displacement has the advantages that it is symmetric with respect to the two structures to be compared, that it varies smoothly upon smooth distortions of either or both of the structures, and that there is no need for a user-defined parameter such as the number of molecules used for the comparison. Note that the COMPACK algorithm (Chisholm & Motherwell, 2005), as implemented in *Mercury*, compares atomic coordinates without taking into account the differences in the unit-cell parameters and thus yields different RMSCD values.

In 2017, we determined how well 200 crystal structures were reproduced upon four repeated energy minimizations from slightly different starting points (Hempler *et al.*, 2017). We established that the average discrepancy between two energy minimizations was an RMSCD of 0.0045 Å, although this was not explicitly reported in the article.

Based on a set 225 single-crystal X-ray structures, we previously established that correct structures distort with an average RMSCD of only 0.084 Å when energy minimized with the unit cell free, while RMSCD values greater than 0.25 Å indicate an error in the experimental crystal structure (van de Streek & Neumann, 2010). Crystal structures determined from powder diffraction data are less accurate and, for a set of 215 such crystal structures, we found that correct structures may have RMSCD values of up to 0.35 Å (van de Streek & Neumann, 2014).

When assessing whether an input crystal structure distorted significantly upon geometry optimization, it is important to note that there is no linear relationship between the distortion, the energy and the correctness of a crystal structure. Whereas a correct crystal structure can generally be easily identified

based on a single energy minimization, a large distortion does not imply a major issue. Indeed, very minor issues in a crystal structure, such as an incorrect orientation of an –OH group, can lead to large distortions and large energy differences. Conversely, a small distortion does not necessarily imply that the crystal structure model is close to correct as there may be multiple offsetting contributions. This makes hunting for mistakes in crystal structures a challenge.

An analogous problem to comparing *in silico* and experimental crystal structures is deciding whether a pair of crystal structures are the same form or different polymorphs. There is an extensive literature on this subject (Sacchi *et al.*, 2020; Mayo *et al.*, 2022; Mayo & Johnson, 2025) and, in many cases, no DFT calculations are required to make a conclusive determination. However, energy minimizations may be helpful to resolve the question of same *versus* different in edge cases where COMPACK or powder-difference comparisons yield ambiguous or contradictory results. If one aims to determine if two similar crystal structures are actually the same form, it is greatly advantageous to first generate slightly distorted unit cells using the average of the two sets of lattice parameters prior to fixed-cell energy minimization, as this allows for the DFT energy minimizations to converge to identical, as opposed to merely similar, structures. Establishing that two crystal structures are identical is easier than quantifying similarity.

Comparing an experimental crystal structure before and after energy minimization is trivial because the unit-cell setting, space-group setting and definition of the asymmetric unit, and even the order of the individual atoms, are all guaranteed to be identical. The two crystal structures can, therefore, be compared without any prior alignment. The same is not true when comparing two arbitrary crystal structures of the same compound, or even of the same polymorph. In cases of missed symmetry, symmetry-breaking phase transitions and triclinic unit-cell angles very close to 90°, there is no guarantee that reducing the two (or more) unit cells to their standard settings leads to the same origin and orientation for all crystal structures, and finding the corresponding transformation relating the two (or more) structures can be time consuming.

Simulated powder diffraction patterns have the advantage that they are one-dimensional and have a fixed origin; in other words, simulated powder diffraction patterns can always be compared directly without the need for a prior alignment step. Furthermore, simulated X-ray powder diffraction patterns are, by definition, relatively immune to common crystallographic errors from X-ray diffraction experiments. These include misplaced H atoms, missed symmetry and incorrect element assignments such as C instead of N. However, temperature or pressure differences and energy minimization all cause minor anisotropic differences in the unit-cell parameters, leading to peak shifts in the simulated powder diffraction patterns. Point-by-point measures for powder diffraction profiles, such as R_{wp}, are very sensitive to minor differences in peak positions and, thus, should not be used to quantify the similarity of two simulated powder diffraction patterns. Several similarity measures for powder diffraction patterns account for peak shifts (Otero-de-la-Roza, 2024; Mayo *et al.*, 2022; Habermehl *et al.*, 2014; van de Streek & Motherwell, 2005), which can be described as special cases of the normalized weighted cross-correlation of the two powder diffraction patterns (de Gelder *et al.*, 2001). For the overlay shown in Fig. 1, the normalized weighted cross-correlation value of the simulated powder diffraction patterns with triangle value $l = 3.0°$ 2θ is 0.986.

To assess the effect of temperature on similarity measures, we consider an extreme example. Bond (2021) published a survey of thermal unit-cell expansion coefficients in the CSD and found that the thermal expansion of refcode family BIJWAS is exceptionally large. BIJWAS01 (Rogers & Green, 1986) was determined at room temperature, which is the most common temperature for PXRD measurements, whereas BIJWAS02 (Rogers & Richards, 1987) was determined at 123 K, which is a common temperature for single-crystal measurements. After energy minimization, the structures are indistinguishable. The overlays of the experimental structures and their energy-minimized counterparts are shown in Fig. S6 (see supporting information). With COMPACK, which compares the Cartesian atomic coordinates while ignoring the unit-cell parameters, the RMSCD values are 0.35 and 0.10 Å for the RT and LT structures, respectively. The RMSCD, as defined by Neumann & Perrin (2005), yields 0.18 and 0.075 Å for the RT and LT structures, respectively. The normalized weighted cross-correlation values of the simulated powder diffraction patterns with triangle value $l = 3.0°$ 2θ are 0.935 and 0.997, respectively, *cf.* the values for axitinib Form XLI, determined at room temperature.

5. Guiding principles

The preceding sections dealt with the comparably straightforward tasks of energy optimizing and comparing crystal structures (atomic coordinates and unit-cell parameters); calculating and comparing crystal energies generally requires more thought and is described in the next two sections.

5.1. Structures converge faster than energies with increasing method quality

It is very well established in the field of computational chemistry that molecular geometries are much less sensitive to the chosen level of theory than are electronic energies. Similarly, crystal structures (unit-cell parameters and atomic coordinates) converge faster and are much easier to reproduce than energies. As a consequence, decisions that can be made based on the reproduction of experimental unit-cell parameters and non-H atomic positions by alternative crystal structure models (*e.g.* with differing H-atom positions) may be more reliable than the comparison of small energy differences.

In the following, we will illustrate how to make use of the more rapid convergence of crystal geometries to reduce computational cost. Various combinations of density functionals and basis sets will be written using the method/basis notation; examples of small and large basis sets would be

'lightdense(r)' and 'tight', respectively. With this notation, crystal energies calculated with PBE+D/small and PBE0+D/small, or with PBE+D/small and PBE+D/large, may be quite different. However, energy-minimized crystal structures obtained with PBE+D/small and PBE0+D/large are hardly distinguishable. For the particular example of axitinib Forms I, IV, VI, XXV and XLI, the RMSCD values between the crystal structures energy minimized with PBE+D/lightdense and PBE0+D/lightdense are 0.034, 0.032, 0.033, 0.027 and 0.021 Å, respectively (see Fig. 2).

The energy potential used for the energy minimization (DFT functional, dispersion correction, basis set and *k*-points) can be completely independent of the energy potential applied for the calculation of the single-point energies. Thus, it is recommended to energy minimize crystal structures with PBE+D/small, and to subsequently add a cheap single-point energy calculation with the superior PBE0+D/large method, rather than performing very expensive PBE0+D/large geometry optimizations, as illustrated in Fig. 3(*a*). In comparison, Fig. 3(*b*) shows the very different behaviour of PBE+D and PBE0+D energies.

While the memory and CPU demands of a single-point calculation with PBE0 with a large basis set can still be prohibitive, such a calculation can be further simplified by splitting it into multiple single-point calculations by considering each of them a correction that is added to a cheaper reference energy. For example, the PBE0+D/large energy can be reliably approximated as

$$\begin{aligned} E(\text{PBE+D/large}) \approx\ & E(\text{PBE+D/small}) + \\ & [E(\text{PBE0+D/small}) - E(\text{PBE+D/small})] + \\ & [E(\text{PBE+D/large}) - E(\text{PBE+D/small})] \end{aligned} \tag{3a}$$

where E(PBE+D/small) is the reference energy obtained from a single-point calculation with the energy method PBE+D/small. The first correction is the difference between PBE0+D and PBE+D, while the second is the difference between the large and small basis set. Each of the correction terms improves one aspect of the reference method at a time, as graphically shown in Fig. S7. The above result can also be written as

$$\begin{aligned} E(\text{PBE0+D/large}) \approx\ & E(\text{PBE0+D/small}) + \\ & [E(\text{PBE+D/large}) - E(\text{PBE+D/small})] \end{aligned} \tag{3b}$$

but Equation (3a) shows the symmetry between the individual corrections, allows the individual corrections to be quantified separately, and makes it more obvious how to extend the equation to include additional correction terms.

Within the 0 K approximation, PBE0+D energies are currently the state of the art for intermolecular interactions. Conformational energies, on the other hand, can still be improved by additional single-point calculations on the individual component molecules that form the crystal, called a monomer correction or a single-molecule correction, with either dispersion-corrected second-order Møller–Plesset perturbation theory (MP2D) or range-separated hybrid functionals. ωB97X+D (Chattopadhyay *et al.*, 2025) is one such range-separated hybrid that provides a good balance of accuracy and computational cost; for easier typesetting, ωB97X is sometimes written as wB97X. Such isolated-molecule calculations typically use Gaussian basis sets, which should be of at least triple-ζ quality and ideally include diffuse functions to ensure accurate conformational energies. For the example of MP2D, the calculation is as follows:

$$\begin{aligned} E_{\text{crystal}}(\text{PBE0+D/large \& MP2D}) = {} & E_{\text{crystal}}(\text{PBE0+D/large}) \\ & + \frac{1}{N}\sum_{i=1}^{N}\left[E_{\text{molecule},i}(\text{MP2D}) - E_{\text{molecule},i}(\text{PBE0+D/large})\right] \end{aligned} \tag{4}$$

where the sum runs over all molecules within the unit cell. Note that, if the single-point energy of the crystal is approximated as a linear combination of multiple single-point energies [as in Equation (3)], the single-point energies of the isolated molecules should be evaluated in the same fashion before they are subtracted from the MP2D molecular energy.

5.2. Exploit error cancellation in the computation of relative energies

Energy does not have a natural zero point and it is therefore not possible to refer to 'the' energy of a crystal structure, only to energy differences. The use of relative, as opposed to absolute, energies allows one to make significant use of error cancellation when performing QM calculations. In the context of this article, error cancellation exclusively refers to the cancellation of errors as a result of considering energy differences only (and not the other type of error cancellation arising when two shortcomings in a computational method have opposing effects). As an example, even though the PBE functional is poor in describing the energies involved in breaking and forming bonds, energy differences between polymorphs can be calculated with much greater accuracy

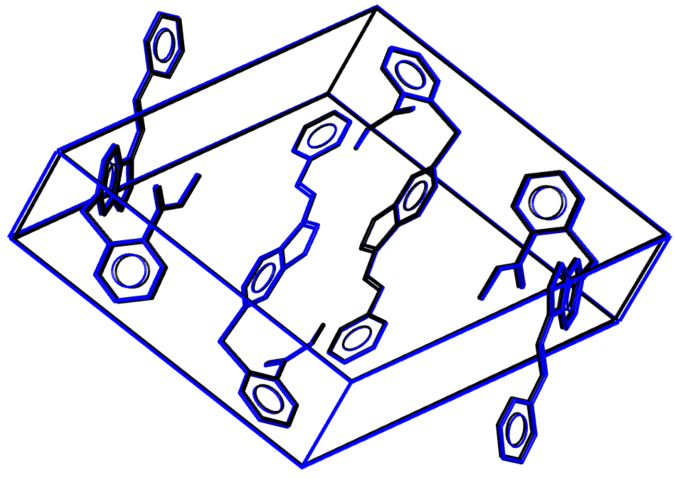

Figure 2
Overlay of the crystal structure of Form XLI of axitinib energy minimized with PBE+D (blue) and energy minimized with PBE0+D (black); RMSCD = 0.021 Å. Whereas the energies may be significantly different, the atomic coordinates and unit-cell parameters from GGA functionals such as PBE and hybrid functionals such as PBE0 are essentially the same. LDA functionals (not shown) are not suitable and lead to distortions.

than molecular formation energies. This is the case because the errors in the molecular formation energies are the same in both polymorphs and offset when considering energy differences.

Error cancellation becomes an even more important factor when comparing two alternative models for a crystal structure, for example, to check the correct orientation of an acetyl group in a crystal structure determined from medium-quality powder diffraction data. The calculated energy difference between two such competing models can be expected to be much more reliable than the calculated energy difference between two arbitrary experimental polymorphs due to their high degree of structural similarity. As a general rule, the more similar the crystal structures, the greater the error cancellation. For example, computed energy differences between polymorphs with the same hydrogen-bonding pattern will be more accurate than energy differences between polymorphs with different hydrogen-bonding schemes.

5.3. Compare the signal to the error bar

An area that is all too often ignored is the question of the error bars, as several different error sources affect calculated energies. By far the smallest, and negligible compared to all other error sources, is the numerical error; it is the computational equivalent of what is called *precision* in experiment, *i.e.* it refers to the reproducibility when an energy minimization on the same crystal structure is repeated multiple times from slightly different starting points. The standard deviation of the atomic coordinates due to numerical error is *ca* 0.0045 Å (see above) and, for energy differences, these errors should contribute well below 0.1 kcal mol^{-1}, and usually less than 0.05 kcal mol^{-1}.

There are relatively few reliable benchmarks available to assess the accuracy of DFT methods for absolute and relative lattice energies of molecular crystals, with the most notable being the X23 (Otero-de-la-Roza & Johnson, 2012*a*; Reilly & Tkatchenko, 2013; Dolgonos *et al.*, 2019) and ICE13 (Brandenburg *et al.*, 2015; Della Pia *et al.*, 2024) data sets. In 2023, we published what to the best of our knowledge is the first comparison of calculated temperature-dependent free-energy differences *versus* experimental free-energy differences (Firaha *et al.*, 2023). These free energies included a single-point correction with PBE0+D for the crystal energy, an MP2D correction for the molecular energy, and the contribution of the phonons calculated using the supercell method. For molecular crystal structures of chemical compounds containing up to 50 atoms (including H atoms), the 0 K PBE+D energy differences between energy-minimized crystal structures have an error bar of about 0.75 kcal mol^{-1}; this error bar is the *accuracy* of the calculated energy differences compared to experiment. A 0 K single-point calculation with PBE0+D on the energy-minimized crystal structures reduces the error bar to about 0.50 kcal mol^{-1}, but a PBE0 single-point calculation takes about one order of magnitude more resources (computer memory and CPU time) than a PBE single-point calculation.

Adding the contribution from the phonons reduces the error bar to about 0.25 kcal mol^{-1}. This means that the error in the calculated energy difference between two molecular crystal structures due to the neglect of temperature is approximately 0.25 kcal mol^{-1}. This is consistent with the results of Nyman & Day (2015), who found that for 70% of pairs of experimental polymorphs, the phonon contribution to the free energies ($|\Delta F_{\rm vib}|$) is smaller than 0.25 kcal mol^{-1}. However, phonon calculations require about two orders of magnitude more resources than a PBE single-point calculation and are

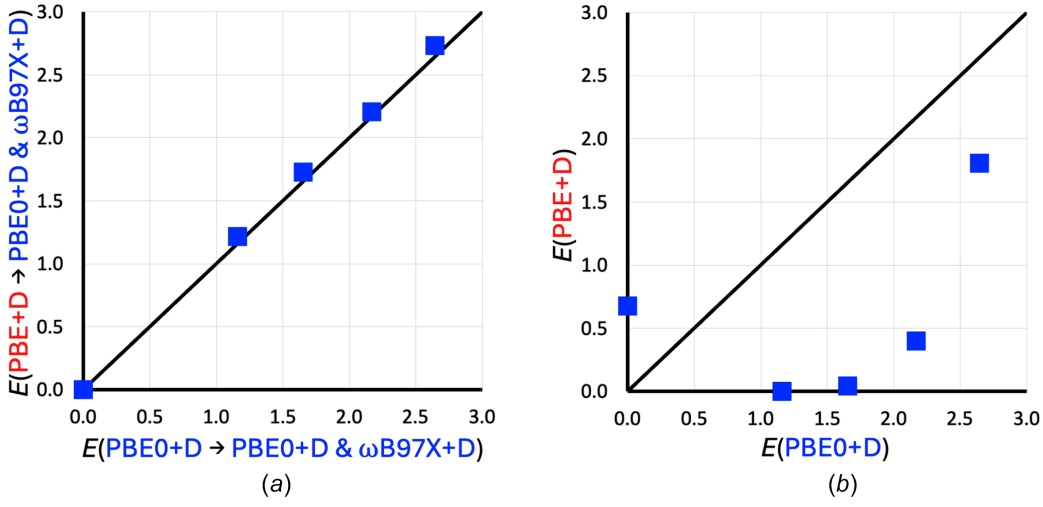

Figure 3
(*a*) The expensive PBE0+D/tight & ωB97X+D single-point energies of five axitinib polymorphs after energy minimization with the cheap PBE+D/lightdense method (*y* axis) and the expensive PBE0+D method (*x* axis). The line $y = x$ is drawn to guide the eye. A cheap energy minimization followed by an expensive single-point energy calculation gives the same results as an expensive energy minimization followed by an expensive single-point energy calculation. (*b*) The relative energies of the same five axitinib polymorphs obtained with the cheap PBE+D method (*y* axis) and expensive PBE0+D method (*x* axis). Whereas the PBE+D and PBE0+D structures are almost indistinguishable, the PBE+D and PBE0+D energies are very different. The line $y = x$ is drawn to guide the eye.

beyond the scope of this article. For more sophisticated free energy calculations on molecular crystal structures, the articles by Hunnisett *et al.* (2024), Firaha *et al.* (2023) and Wood *et al.* (2026), and references therein, are good starting points.

5.4. If an energy difference is unexpected, the higher-energy structure is likely in error

Occasionally, a reasonable expectation value for the sign of an energy difference is available, for example, from competitive slurry experiments. If the computationally predicted stability order is substantially opposite to that expected, it is almost always the energy that is higher than expected that is the problem. The reasoning is simple: if a small change to a structural model were to lower the energy of the structure, nature would already have selected the structure with the lower energy. Any change to a correct model is therefore expected to increase the energy; this is merely another application of the Anna Karenina principle. Incorrect models have energies that are systematically higher than expected, and correcting the model lowers the energy, aligning the energy with the expectation.

An excellent example is the case of morphine HCl trihydrate (CSD refcode MORPHC; Gylbert, 1973), the structure of which was investigated computationally by Braun *et al.* (2014). The authors found that the crystal structure distorted upon energy minimization, indicative of a likely error, and the calculated lattice energy was higher than expected. The structure was solved in 1973 and contains one O—H···H—O interaction and one O···Cl^- interaction, with the proton positions assigned to chemically unlikely positions by the crystallographer. Reshuffling the protons results in one O—H···O hydrogen bond and one O—H···Cl^- hydrogen bond, lowering the energy of the trihydrate by 14.1 kcal mol^{-1} (at the PBE+D level) and resolving the problem that the trihydrate was calculated to be highly unstable with respect to the anhydrate (see Fig. S8 in the supporting information).

5.5. Experimental unit-cell parameters are reliable independent of the atomic coordinates

In Rietveld refinement, also called whole-profile fitting, all data points are used in the refinement of the unit-cell parameters and the peak positions are generally only affected by one error, namely, the 2θ zero-point error, which can trivially be modelled. The atomic coordinates, on the other hand, are determined by the intensities, which suffer from much more severe errors, namely, peak overlap and preferred orientation, which are much harder to model. As a result, the experimental unit-cell parameters from X-ray and neutron single-crystal data after about 1980, and from X-ray and neutron powder diffraction data, are highly accurate, even if the coordinates of one or more of the atoms is not. Note that the same is not necessarily true for electron diffraction, where the unit cell is determined with lower precision than X-ray diffraction (Gemmi *et al.*, 2026).

If a centre of symmetry has been overlooked in the determination of a single-crystal structure, this leads to singularities in the refinement and the atomic positions are unreliable (Schomaker & Marsh, 1979), but the unit-cell parameters are not affected. For example, the crystal structure of CSD refcode PASQAB (Konarev *et al.*, 1997) was published in *Cm*, $Z' = \frac{1}{2}$, and the C—C bond lengths in the fullerene molecule range between the unphysically short and long distances of 1.04 and 1.84 Å (see Fig. S9). However, the correct space group is *C*2/*m*, $Z' = \frac{1}{4}$. After averaging the symmetry-equivalent atoms in the corrected space group, the spread is still 1.23 to 1.62 Å, and Marsh *et al.* (2002) writes 'further refinement is clearly needed'. DFT energy minimization is not affected by the missing centre of symmetry, and in our energy-minimized DFT structure in the incorrect space group *Cm*, $Z' = \frac{1}{2}$, the bond lengths are between the much more reasonable values of 1.40 and 1.46 Å (see Fig. S9). In the absence of further experimental data, the best structural model, with reasonable bond lengths for all molecules and including all H atoms, is the result of a DFT energy minimization in *C*2/*m*, $Z' = \frac{1}{4}$ with the experimental unit cell fixed.

5.6. The more additional degrees of freedom, the lower the energy

It should not be necessary to mention this explicitly in a scientific publication, but we have seen cases where, in the comparison of two models, the one with additional degrees of freedom was selected as correct because it had a numerically better figure of merit, such as a more favourable energy. Per the variational principle, additional degrees of freedom will lower the energy, or at least result in it staying the same. However, it is possible that the structure with a higher DFT energy may be a better match to an experimental crystal structure due to neglect of thermal effects or errors inherent in the density functional.

6. Special cases

6.1. Comparing energies of different chemical compounds

Only energies of crystal structures with the same chemical composition can be compared. As we restrict ourselves to the solid state, this means that only polymorphs (and cocrystals of the same stoichiometry) can be compared in practice. To compare the energies of cocrystals of different stoichiometries, the chemical compositions must be balanced; see, for example, Cruz-Cabeza *et al.* (2008) and Taylor & Day (2018).

To compare the energies of crystal structures corresponding to different hydration states, the composition must be balanced either with ice at 0 K (which is a poor approximation for water vapour) or with isolated water molecules (for which there is no hydrogen bonding, prohibiting the error cancellation required for more accurate relative energies). Further, note that the relative stability of different hydration states is properly a function of the relative humidity, so any energy comparison of different hydration states in which the energy of pure water is a constant cannot be expected to capture reality. For a proper computational comparison of the free energies of different hydration states, see Firaha *et al.* (2023).

6.2. Racemic *versus* enantiopure phases

Thermodynamically, the *R* enantiomer, the *S* enantiomer and the racemate of a chiral compound are three different chemical compounds, but no chemical bonds are broken or formed and the energies can therefore be compared as if they were polymorphs. The crystal structures of the *R* enantiomer and the *S* enantiomer are expected to be each other's mirror image, so their energies should be identical and calculations on only one enantiomer need be performed. However, the racemate will, in most cases, have a different crystal structure and must be considered separately.

The racemate can crystallize in space groups with an improper symmetry element (a symmetry element that turns a left hand into a right hand), whereas an enantiomerically pure compound cannot. A racemate therefore has more options available when crystallizing than an enantiopure compound. If the racemate has not crystallized in one of the Sohncke space groups (or, to be pedantic, has not crystallized in a Sohncke space group with $Z' = 2$ with the two molecules in the asymmetric unit having opposite chirality), *i.e.* if the racemate has not crystallized as a so-called conglomerate, one would therefore expect that it has exploited this additional degree of freedom and that its crystal energy is lower (at the same temperature and pressure). Cases where both racemic and conglomerate phases of the same crystal can be obtained experimentally provide excellent benchmarking data to assess the accuracy of computational methods such as DFT, as the relative free energies of the two forms can be determined with high precision from experimental measurements of the enantiomeric excess at the eutectic point (Otero-de-la-Roza *et al.*, 2014*a*; Buchholz *et al.*, 2017).

6.3. Deuteration

^{2}H (deuterium) is twice as heavy as ^{1}H (protium), which changes the vibrations and thereby the atomic equilibrium positions and the crystal free energy; because of zero-point vibrations, this is the case even at 0 K. In 0 K DFT calculations, in which vibrations do not play a role, the atomic positions, electron densities and electronic energies are exactly identical by definition. Experimentally, the differences in positions of ^{2}H and ^{1}H atoms are very small, even for perdeuterated compounds. This results in electron densities, powder X-ray diffraction patterns, unit-cell parameters and atomic coordinates for deuterated and non-deuterated compounds that are to all intents and purposes identical. However, some exceptions are known (Merz & Kupka, 2015) and, in those cases, 0 K DFT calculations cannot be used to reproduce or predict the energy differences.

6.4. Salts *versus* cocrystals

The PBE functional incorrectly favours salts over cocrystals (LeBlanc *et al.*, 2018). In our experience, there is often virtually no energy barrier between the salt and the cocrystal forms, *i.e.* the proton's energy potential is a single well, not a double well. This means that energy minimization will typically yield the same final structure (salt or cocrystal), regardless of the starting structure (salt or cocrystal). It is therefore not possible to calculate improved energies for both models to decide which is more stable, and the energy calculations as described in this article cannot be used to address the question if a crystal structure is a salt or a cocrystal. Moreover, in resonance-assisted hydrogen bonds (Dračínský *et al.*, 2015; Štoček *et al.*, 2022), the H atoms are delocalized and can only be properly described by a dynamic model and not a static structure from energy minimization. However, as the non-H atoms are not affected by such a dynamic proton exchange, the distortion of a crystal structure model upon energy minimization as quantified by the RMSCD of the non-H atoms can still be used as a measure for the correctness of a crystal structure.

The distinction between a salt and a cocrystal is very important for the pharmaceutical industry, yet the low X-ray scattering power of a H atom can complicate the experimental distinction *via* X-ray diffraction. The computational determination of the proton position is therefore an active area of research (Abramov & Wang, 2024; Bal & Collas, 2024; Beran, 2025) but beyond the scope of this best practice guide.

6.5. Isomers and diastereomers

PBE+D can give significant errors for the relative energies of chemical isomers, even in cases such as differences between linear and branched alkanes, in which the numbers and types of all atoms and bonds are conserved, such that the interconversion reaction between the isomers would be isodesmic (Goerigk *et al.*, 2017). However, if two (or more) molecules are sufficiently similar, error cancellation can facilitate comparison of their lattice energies. For example, to show that the differences in their melting points were caused by the contributions of their molecular symmetries to their entropies, the lattice energies of three tribromobenzene isomers were calculated and compared (van de Streek, 2022), relying on their chemical similarity to maximize error cancellation.

Additionally, diastereomers, unlike enantiomers, are chemically distinct compounds so their energies cannot be directly compared. However, diastereomers are a subset of structural isomers where the bonding is maximally conserved and only the arrangements about two or more stereocentres differ, so error cancellation will reduce PBE+D errors in the relative single-molecule energies.

6.6. Tautomers

In the crystal structures of tautomers, the positions of the H atoms in the individual crystal structures are generally unambiguous and are reproduced very well by PBE+D energy minimizations (Fig. S10). Comparison of the energies of crystal structures consisting of the same tautomer should be no different from any other crystal energy calculation. Problems arise when the crystal energies of structures consisting of different tautomers are compared: the inherent energy errors of the PBE+D and PBE0+D functionals when bonds are broken and formed are often greater than the energy differences between polymorphs. As a bare minimum, the

meaningful comparison of the energies of polymorphs containing different tautomers requires not only a PBE0 single-point energy correction, but also an MP2D or ωB97X+D monomer correction. Fig. S11 shows the PBE+D/small crystal energies, PBE0+D/large crystal energies, ωB97X+D molecular energies and PBE0+D/large & ωB97X+D crystal energies for thiobarbituric acid Form II (PABNAJ, enol tautomer), Form IV (PABNIR, 1:1 keto–enol tautomers) and Form III (THBARB01, keto tautomer) (Chierotti *et al.*, 2010), illustrating the poor performance of the PBE and PBE0 functionals for the energy differences between tautomers. More sophisticated quantum-mechanical methods may be needed for a more general approach to the modelling of the energies of tautomers (Perry *et al.*, 2025).

Determining the correct tautomer for a crystal structure model is still possible if the appropriate metrics are considered, as illustrated for the CSD entry NILVEL (Nfor *et al.*, 2013). Here, inspection of the hydrogen bonds with *Mercury* reveals two non-bonded N···N contacts of 2.907 Å; in the absence of a H atom, this implies a short contact between two lone pairs, which is highly unlikely. Upon energy minimization with PBE+D, the RMSCD is 0.84 Å, whereas the RMSCD for a model corresponding to an alternative tautomer is only 0.11 Å (Figs. S12 and S13). As the low RMSCD alone is sufficient to be confident in structural assignment, more sophisticated energy calculations are not needed, although the PBE+D energy difference between the two models (19.1 kcal mol^{-1} in favour of the alternative tautomer) is also consistent with the geometry argument.

7. Examples

7.1. Example I: confirming the paroxetine HCl 0.9-hydrate structure

The crystal structure of paroxetine HCl hemihydrate was a late-appearing phase, displacing the thermodynamically less stable paroxetine HCl 0.9-hydrate, and the two forms were the subject of a patent battle (Bučar *et al.*, 2015). Only one crystal structure for paroxetine HCl 0.9-hydrate, determined from synchrotron powder diffraction data, is present in the CSD (CSD refcode EHOXEE; Howard *et al.*, 2003). As this crystal structure was submitted as a *CSD Communication*, there was no associated peer-reviewed publication and no associated publicly available experimental powder diffraction data or plot of the Rietveld refinement. The experimental powder diffraction data was not deposited with the International Center for Diffraction Data (IDD) either. Thus, we turned to DFT modelling to confirm or dispute the deposited crystal structure.

While the H atoms of the water molecule are not present in the CSD structure, their approximate positions are obvious and were added using an in-house C++ code. In the calculations, the occupancy of the water molecule is exactly 1.0 rather than 0.9, and only additional experimental data can determine the exact occupancy. We then energy minimized the experimental structure, including the unit-cell parameters. The resulting RMSCD in the non-H-atom positions is 0.20 Å (see Fig. S14), from which we conclude that the experimental structure is most likely correct. As unit-cell parameters from PXRD are generally accurate, we can prepare a reliable model of the experimental structure, including H atoms, by keeping the unit-cell parameters at their experimental values and energy minimizing the atomic coordinates.

7.2. Example II: pyrazine-ring rotation in glipizide

The crystal structure of glipizide was determined from laboratory powder X-ray diffraction data (Burley, 2005). Two orientations are possible for the pyrazine ring, differing only in the exchange of a CH group and an N atom, both representing seven electrons. Burley commented on the two possibilities in the article and chose one at random. To confirm or refute this choice, both models were energy minimized with PBE+D with the unit-cell free. The model as published distorts with an RMSCD of 0.72 Å [Fig. S15(*a*)], while the alternative model hardly distorts with an RMSCD of 0.13 Å [Fig. S15(*b*)] and has a crystal energy that is 4.6 kcal mol^{-1} more favourable. This leads us to conclude that the alternative model is actually correct. A Rietveld refinement with polymorph-dependent restraints against the original experimental data is shown in Fig. S16.

7.3. Example III: determining H-atom positions in riboflavin

Riboflavin contains four hydroxyl groups and there are multiple possible arrangements for the hydrogen-bond network. The crystal structure was determined from synchrotron powder X-ray diffraction data and the authors compared the energies of several hydrogen-bonding patterns from DFT calculations with the unit cell fixed (CSD refcode XARWUM; Guerain *et al.*, 2021). The published hydrogen-bonding pattern looks plausible and satisfies all hydrogen-bond donors. Moreover, when the unit cell is kept fixed, the RMSCD of the published structure upon energy minimization is only 0.23 Å [Fig. S17(*a*)]. However, energy minimization with the unit cell free provides additional degrees of freedom, allowing for a large distortion of the unit cell, with an RMSCD of 0.54 Å [Fig. S17(*b*)]. One of the hydroxyl groups can be rotated by 180°, turning a OH···O=C hydrogen bond and a chain of OH···OH···O=C hydrogen bonds into one chain of concerted OH···OH···OH···O=C hydrogen bonds. The RMSCD after energy minimization with the unit cell free is then only 0.13 Å [Fig. S17(*c*)] and is 0.86 kcal mol^{-1} more stable than the distorted structure. A Rietveld refinement of the corrected hydrogen-bonded structure with polymorph-dependent restraints against the original experimental data is shown in Fig. S18. After energy minimization with the unit-cell parameters fixed at their published values, the energy difference between the published and the corrected crystal structure models is 4.3 kcal mol^{-1}.

Acknowledgements

ERJ thanks the Natural Sciences and Engineering Research Council (NSERC) of Canada and the Royal Society for

financial support *via* their Discovery Grants and Wolfson Visiting Fellowship programmes, respectively.

References

Abramov, Y. A. & Wang, J. (2024). *Cryst. Growth Des.* **24**, 4017–4024.
Adamo, C. & Barone, V. (1999). *J. Chem. Phys.* **110**, 6158–6170.
Bal, K. M. & Collas, A. (2024). *CrystEngComm* **26**, 6765–6773.
Becke, A. D. (1986). *J. Chem. Phys.* **85**, 7184–7187.
Becke, A. D. (1993). *J. Chem. Phys.* **98**, 1372–1377.
Becke, A. D. & Johnson, E. R. (2007). *J. Chem. Phys.* **127**, 154108.
Beran, G. J. O. (2025). *Chem. Sci.* **16**, 23026–23037.
Blum, V., Gehrke, R., Hanke, F., Havu, P., Havu, V., Ren, X., Reuter, K. & Scheffler, M. (2009). *Comput. Phys. Commun.* **180**, 2175–2196.
Boldyreva, E. V., Shakhtshneider, T. P., Vasilchenko, M. A., Ahsbahs, H. & Uchtmann, H. (2000). *Acta Cryst.* B**56**, 299–309.
Bond, A. D. (2021). *Acta Cryst.* B**77**, 357–364.
Bond, A. D., Solanko, K. A., van de Streek, J. & Neumann, M. A. (2011). *CrystEngComm* **13**, 1768–1771.
Brandenburg, J. G., Maas, T. & Grimme, S. (2015). *J. Chem. Phys.* **142**, 124104.
Braun, D. E., Gelbrich, T., Kahlenberg, V. & Griesser, U. J. (2014). *Mol. Pharm.* **11**, 3145–3163.
Bryenton, K. R., Adeleke, A. A., Dale, S. G. & Johnson, E. R. (2023). *WIREs Comput. Mol. Sci.* **13**, e1631.
Bučar, D.-K., Lancaster, R. W. & Bernstein, J. (2015). *Angew. Chem. Int. Ed.* **54**, 6972–6993.
Buchholz, H. K., Hylton, R. K., Brandenburg, J. G., Seidel-Morgenstern, A., Lorenz, H., Stein, M. & Price, S. L. (2017). *Cryst. Growth Des.* **17**, 4676–4686.
Bujak, M., Podsiadło, M. & Katrusiak, A. (2021). *Acta Cryst.* B**77**, 632–637.
Burley, J. C. (2005). *Acta Cryst.* B**61**, 710–716.
Bursch, M., Mewes, J.-M., Hansen, A. & Grimme, S. (2022). *Angew. Chem. Int. Ed.* **61**, e202205735.
Caldeweyher, E., Mewes, J.-M., Ehlert, S. & Grimme, S. (2020). *Phys. Chem. Chem. Phys.* **22**, 8499–8512.
Campeta, A. M., Chekal, B. P., Abramov, Y. A., Meenan, P. A., Henson, M. J., Shi, B., Singer, R. A. & Horspool, K. R. (2010). *J. Pharm. Sci.* **99**, 3874–3886.
Chattopadhyay, A., Hill, A. R., Wright, S. E., Beran, G. J. O. & Cruz-Cabeza, A. J. (2025). *J. Am. Chem. Soc.* **147**, 39192–39203.
Chierotti, M. R., Ferrero, L., Garino, N., Gobetto, R., Pellegrino, L., Braga, D., Grepioni, F. & Maini, L. (2010). *Chem. Eur. J.* **16**, 4347–4358.
Chisholm, J. A. & Motherwell, S. (2005). *J. Appl. Cryst.* **38**, 228–231.
Clark, S. J., Segall, M. D., Pickard, C. J., Hasnip, P. J., Probert, M. I. J., Refson, K. & Payne, M. C. (2005). *Z. Kristallogr. Cryst. Mater.* **220**, 567–570.
Cruz-Cabeza, A. J., Day, G. M. & Jones, W. (2008). *Chem. Eur. J.* **14**, 8830–8836.
de Gelder, R., Wehrens, R. & Hageman, J. A. (2001). *J. Comp. Chem.* **22**, 273–289.
Della Pia, F., Zen, A., Alfè, D. & Michaelides, A. (2024). *Phys. Rev. Lett.* **133**, 046401.
Dolgonos, G. A., Hoja, J. & Boese, A. D. (2019). *Phys. Chem. Chem. Phys.* **21**, 24333–24344.
Dovesi, R., Erba, A., Orlando, R., Zicovich-Wilson, C. M., Civalleri, B., Maschio, L., Rérat, M., Casassa, S., Baima, J., Salustro, S. & Kirtman, B. (2018). *WIREs Comput. Mol. Sci.* **8**, e1360.
Dračínský, M., Čechová, L., Hodgkinson, P., Procházková, E. & Janeba, Z. (2015). *Chem. Commun.* **51**, 13986–13989.
Feast, G. C., Haestier, J., Page, L. W., Robertson, J., Thompson, A. L. & Watkin, D. J. (2009). *Acta Cryst.* C**65**, o635–o638.
Firaha, D., Liu, Y. M., van de Streek, J., Sasikumar, K., Dietrich, H., Helfferich, J., Aerts, L., Braun, D. E., Broo, A., DiPasquale, A. G., Lee, A. Y., Le Meur, S., Nilsson Lill, S. O., Lunsmann, W. J., Mattei, A., Muglia, P., Putra, O. D., Raoui, M., Reutzel-Edens, S., Rome, S., Sheikh, A. Y., Tkatchenko, A., Woollam, G. R. & Neumann, M. A. (2023). *Nature* **623**, 324–328.
Gemmi, M., Palatinus, L., Boullay, P., Abrahams, J. P., Ben Meriem, A., Cordero-Oyonarte, E., Emerson Agbemeh, V., Chintakindi, H., Faye Diouf, M. D., Filipcik, P., Gemmrich Hernandéz, L., van Genderen, E., Hadermann, J., Hajizadeh, A., Jeriga, B., Kolb, U., Matinyan, S., Passuti, S., Santucci, M., Suresh, A., Pérez, O., Tai, C.-W., Vypritskaia, A., Wang, L., Xu, H. & Zou, X. (2026). *IUCrJ* **13**, 198–210.
Gillan, M. J., Alfè, D. & Michaelides, A. (2016). *J. Chem. Phys.* **144**, 130901.
Goerigk, L., Hansen, A., Bauer, C., Ehrlich, S., Najibi, A. & Grimme, S. (2017). *Phys. Chem. Chem. Phys.* **19**, 32184–32215.
Greenwell, C. & Beran, G. J. O. (2020). *Cryst. Growth Des.* **20**, 4875–4881.
Grimme, S. (2006). *J. Comp. Chem.* **27**, 1787–1799.
Grimme, S., Antony, J., Ehrlich, S. & Krieg, H. (2010). *J. Chem. Phys.* **132**, 154104.
Grimme, S., Ehrlich, S. & Goerigk, L. (2011). *J. Comp. Chem.* **32**, 1456–1465.
Groom, C. R., Bruno, I. J., Lightfoot, M. P. & Ward, S. C. (2016). *Acta Cryst.* B**72**, 171–179.
Guerain, M., Affouard, F., Henaff, C., Dejoie, C., Danède, F., Siepmann, J., Siepmann, F. & Willart, J.-F. (2021). *Acta Cryst.* C**77**, 800–806.
Gylbert, L. (1973). *Acta Cryst.* B**29**, 1630–1635.
Habermehl, S., Mörschel, P., Eisenbrandt, P., Hammer, S. M. & Schmidt, M. U. (2014). *Acta Cryst.* B**70**, 347–359.
Hempler, D., Schmidt, M. U. & van de Streek, J. (2017). *Acta Cryst.* B**73**, 756–766.
Hodge, R. L., Kaduk, J. A., Gindhart, A. M. & Blanton, T. N. (2020). *Powder Diffr.* **35**, 136–143.
Hoja, J., Ko, H.-Y., Neumann, M. A., Car, R., DiStasio, R. A. & Tkatchenko, A. (2019). *Sci. Adv.* **5**, eaau3338.
Howard, J. A. K., Pattison, P. & Chetina, O. (2003). CCDC 210488: Experimental Crystal Structure Determination, doi:10.5517/cc720y7.
Hunnisett, L. M., Francia, N., Nyman, J., Abraham, N. S., Aitipamula, S., Alkhidir, T., Almehairbi, M., Anelli, A., Anstine, D. M., Anthony, J. E., Arnold, J. E., Bahrami, F., Bellucci, M. A., Beran, G. J. O., Bhardwaj, R. M., Bianco, R., Bis, J. A., Boese, A. D., Bramley, J., Braun, D. E., Butler, P. W. V., Cadden, J., Carino, S., Červinka, C., Chan, E. J., Chang, C., Clarke, S. M., Coles, S. J., Cook, C. J., Cooper, R. I., Darden, T., Day, G. M., Deng, W., Dietrich, H., DiPasquale, A., Dhokale, B., van Eijck, B. P., Elsegood, M. R. J., Firaha, D., Fu, W., Fukuzawa, K., Galanakis, N., Goto, H., Greenwell, C., Guo, R., Harter, J., Helfferich, J., Hoja, J., Hone, J., Hong, R., Hušák, M., Ikabata, Y., Isayev, O., Ishaque, O., Jain, V., Jin, Y., Jing, A., Johnson, E. R., Jones, I., Jose, K. V. J., Kabova, E. A., Keates, A., Kelly, P. F., Klimeš, J., Kostková, V., Li, H., Lin, X., List, A., Liu, C., Liu, Y. M., Liu, Z., Lončarić, I., Lubach, J. W., Ludík, J., Marom, N., Matsui, H., Mattei, A., Mayo, R. A., Melkumov, J. W., Mladineo, B., Mohamed, S., Momenzadeh Abardeh, Z., Muddana, H. S., Nakayama, N., Nayal, K. S., Neumann, M. A., Nikhar, R., Obata, S., O'Connor, D., Oganov, A. R., Okuwaki, K., Otero-de-la-Roza, A., Parkin, S., Parunov, A., Podeszwa, R., Price, A. J. A., Price, L. S., Price, S. L., Probert, M. R., Pulido, A., Ramteke, G. R., Rehman, A. U., Reutzel-Edens, S. M., Rogal, J., Ross, M. J., Rumson, A. F., Sadiq, G., Saeed, Z. M., Salimi, A., Sasikumar, K., Sekharan, S., Shankland, K., Shi, B., Shi, X., Shinohara, K., Skillman, A. G., Song, H., Strasser, N., van de Streek, J., Sugden, I. J., Sun, G., Szalewicz, K., Tan, L., Tang, K., Tarczynski, F., Taylor, C. R., Tkatchenko, A., Tom, R., Touš, P., Tuckerman, M. E., Unzueta, P. A., Utsumi, Y., Vogt-Maranto, L., Weatherston, J., Wilkinson, L. J., Willacy, R. D., Wojtas, L., Woollam, G. R., Yang, Y., Yang, Z., Yonemochi, E., Yue, X., Zeng, Q., Zhou, T., Zhou, Y., Zubatyuk, R. & Cole, J. C. (2024). *Acta Cryst.* B**80**, 548–574.

Ibberson, R. M. & Prager, M. (1995). *Acta Cryst.* B**51**, 71–76.
Johnson, E. R. & Becke, A. D. (2006). *J. Chem. Phys.* **124**, 174104.
Johnson, E. R., Wolkow, R. A. & DiLabio, G. A. (2004). *Chem. Phys. Lett.* **394**, 334–338.
Kim, Y., Song, S., Sim, E. & Burke, K. (2019). *J. Phys. Chem. Lett.* **10**, 295–301.
Kokott, S., Blum, V. & Scheffler, M. (2025). *J. Chem. Phys.* **162**, 224103.
Konarev, D. V., Valeev, E. F., Slovokhotov, Y. L., Shul'ga, Y. M. & Lyubovskaya, R. N. (1997). *J. Chem. Res. (S)* pp. 442–443.
Kresse, G. & Furthmüller, J. (1996). *Phys. Rev. B* **54**, 11169.
Kresse, G. & Hafner, J. (1994). *J. Phys. Condens. Matter* **6**, 8245.
LeBlanc, L. M., Dale, S. G., Taylor, C. R., Becke, A. D., Day, G. M. & Johnson, E. R. (2018). *Angew. Chem. Int. Ed.* **57**, 14906–14910.
Lejaeghere, K., Bihlmayer, G., Björkman, T., Blaha, P., Blügel, S., Blum, V., Caliste, D., Castelli, I. E., Clark, S. J., Dal Corso, A., de Gironcoli, S., Deutsch, T., Dewhurst, J. K., Di Marco, I., Draxl, C., Dułak, M., Eriksson, O., Flores-Livas, J. A., Garrity, K. F., Genovese, L., Giannozzi, P., Giantomassi, M., Goedecker, S., Gonze, X., Grånäs, O., Gross, E. K. U., Gulans, A., Gygi, F., Hamann, D. R., Hasnip, P. J., Holzwarth, N. A. W., Iuşan, D., Jochym, D. B., Jollet, F., Jones, D., Kresse, G., Koepernik, K., Küçükbenli, E., Kvashnin, Y. O., Locht, I. L. M., Lubeck, S., Marsman, M., Marzari, N., Nitzsche, U., Nordström, L., Ozaki, T., Paulatto, L., Pickard, C. J., Poelmans, W., Probert, M. I. J., Refson, K., Richter, M., Rignanese, G.-M., Saha, S., Scheffler, M., Schlipf, M., Schwarz, K., Sharma, S., Tavazza, F., Thunström, P., Tkatchenko, A., Torrent, M., Vanderbilt, D., van Setten, M. J., Van Speybroeck, V., Wills, J. M., Yates, J. R., Zhang, G.-X. & Cottenier, S. (2016). *Science* **351**, aad3000.
Macrae, C. F., Sovago, I., Cottrell, S. J., Galek, P. T. A., McCabe, P., Pidcock, E., Platings, M., Shields, G. P., Stevens, J. S., Towler, M. & Wood, P. A. (2020). *J. Appl. Cryst.* **53**, 226–235.
Marsh, R. E., Kapon, M., Hu, S. & Herbstein, F. H. (2002). *Acta Cryst.* B**58**, 62–77.
Mayo, R. A. & Johnson, E. R. (2025). *Advances in Organic Crystal Chemistry: Comprehensive Reviews 2025 on Crystal Structures*, edited by S. Kobatake & H. Uekusa, pp. 195–236. Singapore: Springer Nature Singapore.
Mayo, R. A., Otero-de-la-Roza, A. & Johnson, E. R. (2022). *CrystEngComm* **24**, 8326–8338.
Merz, K. & Kupka, A. (2015). *Cryst. Growth Des.* **15**, 1553–1558.
Nam, S., Cho, E., Sim, E. & Burke, K. (2021). *J. Phys. Chem. Lett.* **12**, 2796–2804.
Neumann, M. A., Leusen, F. J. J. & Kendrick, J. (2008). *Angew. Chem. Int. Ed.* **47**, 2427–2430.
Neumann, M. A. & Perrin, M.-A. (2005). *J. Phys. Chem. B* **109**, 15531–15541.
Nfor, E. N., Husian, A., Majoumo-Mbe, F., Njah, I. N., Offiong, O. E. & Bourne, S. A. (2013). *Polyhedron* **63**, 207–213.
Nichols, G. & Frampton, C. S. (1998). *J. Pharm. Sci.* **87**, 684–693.
Nyman, J. & Day, G. M. (2015). *CrystEngComm* **17**, 5154–5165.
Otero-de-la-Roza, A. (2024). *J. Appl. Cryst.* **57**, 1401–1414.
Otero-de-la-Roza, A., Cao, B. H., Price, I. K., Hein, J. E. & Johnson, E. R. (2014*a*). *Angew. Chem. Int. Ed.* **53**, 7879–7882.
Otero-de-la-Roza, A. & Johnson, E. R. (2012*a*). *J. Chem. Phys.* **137**, 054103.
Otero-de-la-Roza, A. & Johnson, E. R. (2012*b*). *J. Chem. Phys.* **136**, 174109.
Otero-de-la-Roza, A., Johnson, E. R. & Luaña, V. (2014*b*). *Comput. Phys. Commun.* **185**, 1007–1018.
Perdew, J. P., Burke, K. & Ernzerhof, M. (1996*a*). *Phys. Rev. Lett.* **77**, 3865–3868.
Perdew, J. P., Ernzerhof, M. & Burke, K. (1996*b*). *J. Chem. Phys.* **105**, 9982–9985.
Perry, C. J., Ramos, S. A., Phelps, M. C., Mueller, L. J. & Beran, G. J. O. (2025). *J. Am. Chem. Soc.* **147**, 26865–26876.
Price, A. J. A., Otero-de-la-Roza, A. & Johnson, E. R. (2023). *Chem. Sci.* **14**, 1252–1262.
Reilly, A. M. & Tkatchenko, A. (2013). *J. Chem. Phys.* **139**, 024705.
Rogers, R. D. & Green, L. M. (1986). *J. Incl. Phenom.* **4**, 77–84.
Rogers, R. D. & Richards, P. D. (1987). *J. Incl. Phenom.* **5**, 631–638.
Sacchi, P., Lusi, M., Cruz-Cabeza, A. J., Nauha, E. & Bernstein, J. (2020). *CrystEngComm* **22**, 7170–7185.
Schomaker, V. & Marsh, R. E. (1979). *Acta Cryst.* B**35**, 1933–1934.
Štoček, J. R., Socha, O., Císařová, I., Slanina, T. & Dračínský, M. (2022). *J. Am. Chem. Soc.* **144**, 7111–7116.
Taylor, C. R. & Day, G. M. (2018). *Cryst. Growth Des.* **18**, 892–904.
Tejchman, W., Żesławska, E., Zborowski, K., Nitek, W. & Żylewski, M. (2015). *Arkivoc* **2015**, 216–230.
Thompson, H. P. G. & Day, G. M. (2014). *Chem. Sci.* **5**, 3173–3182.
Tkatchenko, A., DiStasio, R. A., Car, R. & Scheffler, M. (2012). *Phys. Rev. Lett.* **108**, 236402.
Tkatchenko, A. & Scheffler, M. (2009). *Phys. Rev. Lett.* **102**, 073005.
van de Streek, J. (2022). *Acta Cryst.* B**78**, 274–275.
van de Streek, J., Dietrich, H., Firaha, D., Ovchinnikov, A., Sasikumar, K. & Neumann, M. A. (2026). In preparation.
van de Streek, J. & Motherwell, S. (2005). *Acta Cryst.* B**61**, 504–510.
van de Streek, J. & Neumann, M. A. (2010). *Acta Cryst.* B**66**, 544–558.
van de Streek, J. & Neumann, M. A. (2014). *Acta Cryst.* B**70**, 1020–1032.
Wang, Y. & Perdew, J. P. (1991). *Phys. Rev. B* **44**, 13298–13307.
Wood, W. P., Arhangelskis, M., Bartůňková, E., Bernardes, C. E. S., Boese, A. D., Braun, D. E., Bučar, D.-K., Butkiewicz, H., Červinka, C., Civalleri, B., Couvrat, N., de Ronde, E., Donà, L., Dračínský, M., Firaha, D., Fulem, M., Geronia, R. II, Goncharova, N., Gryl, M., Hoja, J., Hoser, A., Krzeszczakowska, J., List, A., Lončarić, I., Mladineo, B., Nyman, J., Olehovics, E., Raimondo, M., Rietveld, I. B., Rodrigues, R. I. S., Russo, L., Salvalaglio, M., Sarraguça, M., Šnajdr, J., Štejfa, V., Sun, G., Tinnemans, P., Whitfield, P. S., Yang, Z., Zhang, Y. & Price, S. L. (2026). *Cryst. Growth Des.* **26**, 476–493.
Zhang, Y. & Yang, W. (1998). *Phys. Rev. Lett.* **80**, 890.
Zouev, I., Cao, D.-K., Sreevidya, T. V., Telzhensky, M., Botoshansky, M. & Kaftory, M. (2011). *CrystEngComm* **13**, 4376–4381.